Analyzing Current Trends and forecasting Snow Cover Dynamics: A Multi-Data Approach utilizing Satellite Data, ERA5 and SSP Scenarios for Enhanced Disaster Preparedness

Pramod Kumar M.[1]*, Vazeer Mohammood[2] and Durga Rao K.H.V.[3]
1. Water Resources Group, RSA, National Remote Sensing Centre, Hyderabad, 500037, INDIA
2. College of Engineering, Department of Civil Engineering, Andhra University, Vishakhapatnam, 530003, INDIA
3. DMSG, RSA, NRSC/ISRO, Hyderabad, Telangana, 500037, INDIA
*mpk25189@gmail.com

Abstract
The Indus Himalayan region, characterized by its challenging mountainous terrain, presents obstacles for ground observations. This study aims to investigate variations in Snow Cover Area (SCA) and its relationship with other climatic variables. We utilized MODIS snow cover, temperature, ECMWF ERA-5 and SRTM elevation products to assess present trends (2002-2023) and CMIP6 SSP scenarios (SSP1-2.6, SSP2-4.5, SSP5-8.5) to project future impacts (2024 to 2100) of climate change. Statistical analyses reveal decadal trends in SCA, with slight increases observed in winter, summer, autumn and annual periods (0.14% year^{-1}, 0.33% year^{-1}, 0.45% year^{-1} and 0.35% year^{-1} respectively). A significant positive trend is noted in spring (July-September) at 0.35% year^{-1}. The study indicates an insignificant negative correlation (−0.81) between SCA and Land Surface Temperature (LST), suggesting potential climate change impacts on SCA depletion in the Northwest Himalayan (NWH) region.

By projecting future climate scenarios including changes in temperature, precipitation patterns and annual frost days (Tmin < 0°C) until 2100, we observed a reduction in frost days and increasing temperatures due to climate change. Understanding evolving climate dynamics and snow cover trends is essential for developing effective strategies to address climate change impacts and to ensure community resilience in the Indus Himalayas.

Keywords: MODIS, Snow Cover Area, Northwest Himalayans, Climate Change, Disaster Preparedness.

Introduction

The Himalayan region, often referred to as the ‘Asian Water Tower’, is characterized by extensive snowfields and glaciers that play a pivotal role in regulating hydrological and meteorological conditions[30,31]. Ranking as the third-largest ice mass on Earth after the Arctic and Antarctic regions, the Himalayan snow and ice reserves contribute significantly to major river systems including the Indus, Ganga, Brahmaputra, Yangtze, Yellow and Mekong, sustaining freshwater resources for over 1.4 billion people in the region[2,32]. The dynamic climate of the planet undergoes regular warming and cooling cycles, influencing oceanic and atmospheric circulation patterns that dictate snow accumulation and ablation processes.

Approximately 70% of the planet's freshwater is stored in the form of permanent snow cover and glaciers. Monitoring snow cover in mountainous terrains is challenging using conventional methods, necessitating remote sensing techniques to understand snow cover area (SCA) and their climatic relationships[4,22].

Climate change profoundly impacts mountain hydrology, rendering it more susceptible to variations in precipitation and temperature, which in turn affect snow depth, volume and extent[21]. Snow cover dynamics plays a critical role in the Earth's energy budget and radiation balance, influencing regional meteorological and climatological systems. Previous studies have documented global trends in snow cover extent in response to climate change[5]. Assessing snow cover accurately in mountainous regions like the Himalayas is challenging[20]. Remote sensing, particularly using MODIS (Moderate Resolution Imaging Spectroradiometer), offers a viable solution due to its high temporal resolution and comprehensive spectral coverage[6].

Earlier studies employed multispectral sensors like Landsat and SPOT, but these suffered from limitations such as band saturation and inadequate spatial resolution[19,34]. NOAA satellite data, while possessing high temporal resolution, faces challenges related to spatial resolution and atmospheric effects[18]. MODIS data, with its medium spatial resolution and wide spectral range, has emerged as a preferred choice for snow cover estimation[7]. Land surface temperature (LST) is a key indicator of land surface processes and energy balance, essential for understanding climate dynamics on regional and global scales. LST data derived from satellite observations contributes to various fields including geology, hydrology and vegetation monitoring.

Previous studies have demonstrated the accuracy of MODIS-derived LST products in comparison to other satellite sensors[12,24]. The correlation between LST and snow cover

*** Author for Correspondence**

https://doi.org/10.25303/1711da01013

provides valuable insights for climate change analysis, especially in data scarce Himalayan regions[17,28]. This study focuses on the Northwest Himalayan (NWH) region within the Indus basin, characterized by numerous glaciers and perennial river catchments vital for irrigation and hydropower generation[14,27].

The primary objectives include analyzing decadal variations in snow cover trends, exploring climatic variability using LST, assessing elevation-wise changes in snow cover and correlating with ECMWF ERA5 total precipitation data and understanding future climate change using CMIP6 Shared Sociao Economic Pathways (SSP) scenarios (Climate Change Knowledge Portal: Observed Climate Data, CRU TS4.07 0.5-Degree). Various statistical methods will be employed to detect decadal trends and understand the implications of climate change on snow cover dynamics in this critical region[15,29].

Study area

The study area is located in the Northwest Himalayan (NWH) region, bounded by geographical longitudes 72°E to 81°E and latitudes 30°N to 37°N, as illustrated in figure 1. The elevation ranges from 1024 to 7639 meters above mean sea level (MSL). The Indus basin part of NWH covers a total geographical area of 342,737.88 sq.km, encompassing portions of the Kashmir Himalaya and Himachal Himalaya[1]. This region includes several sub-basins such as Gilgit, Hunza, Indus middle, Astor, Kishanganga, Jhelum, Chenab and others. The slope of NWH varies from north to south[8,35]. The study area receives substantial snowfall from western disturbances[25]. Summer temperatures in the middle Himalayas range from 15°C to 18°C while winter temperatures drop below freezing. Higher elevations above 4800 meters remain permanently snow-covered with sub-freezing temperatures[13].

Material and Methods

SCA and Climate Trend Methods: The snow parameters utilized in this study were derived from the MODIS 8 Daily L3 Global 500 m resolution, Version 6 (MOD10A2.006) products, available from the National Snow and Ice Data Center (NSIDC). These MODIS products are widely recognized and utilized for their high temporal resolution and global coverage, making them valuable for snow cover monitoring. The study period encompassed the hydrological year from September 1st, 2002, to August 30th, 2021, allowing for a comprehensive assessment of long-term snow cover dynamics. Furthermore, MODIS Land Surface Temperature (LST) 1 km resolution 8-day products (MOD11 and MYD11) for the critical melt period (April-June) between 2003 and 2021 were obtained from the USGS Earth Explorer portal, as illustrated in figure 3.

Snow cover extraction involved rigorous analysis of fortnightly, decadal and seasonal variations using advanced statistical techniques. Understanding these variations is essential for assessing climate change impacts on snow cover extent and duration, particularly in sensitive mountainous regions like the Northwest Himalayas[26].

For climate trend analysis, fifth-generation European Centre for Medium-Range Weather Forecasts (ECMWF) Atmospheric Reanalysis data (ERA-5) was utilized. ERA-5 data, provided by the Copernicus Climate Change Service (C3S) at ECMWF, offered detailed climate information on a 0.25° × 0.25° grid from 1979 to the present. This dataset is crucial for identifying long-term climate trends and understanding the broader climatic context impacting snow cover dynamics. Monthly precipitation data covering the period 2001–2023 was sourced from the Copernicus Climate Data Store (CDS). Precipitation plays a critical role in snow accumulation and melt dynamics, making this dataset invaluable for analyzing the hydrological implications of changing precipitation patterns on snow cover[16].

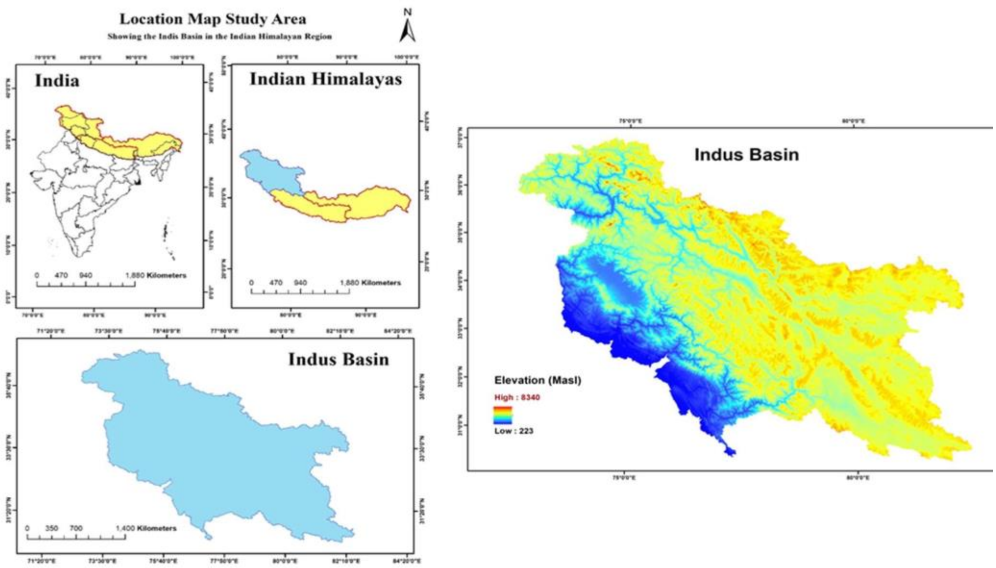

Fig. 1: Geographic Location and Topographic Features of the Indus Basin

Topographic features of the Indus basin were extracted using 1 arc-second (30 m) resolution Shuttle Radar Topography Mission Digital Elevation Model (SRTM-DEM) data tiles obtained from the United States Geological Survey (USGS) Earth Explorer website. These DEM tiles were processed and mosaicked using ArcGIS software to delineate the basin area, as depicted in figure 1. Hypsometric tinting of the study area derived from the SRTM-DEM is presented in figure 3. The comprehensive methodology detailing data acquisition and processing steps is provided through a flowchart and step-by-step procedure, as represented in figure 2. These figures and datasets are essential for elucidating the complex interactions between climate, topography and snow cover dynamics in the Northwest Himalayan region[23].

Analysis of Land Surface Temperature using MODIS Products (MOD11A2 and MYD11A2): Both MOD11A2 and MYD11A2 products are widely used in climate studies, environmental monitoring and research related to land surface processes[9]. They provide valuable information for assessing temperature patterns and changes across different landscapes over time. The MODIS Aqua/Terra LST products with 1 km spatial resolution were obtained for analysis (Figure 3). This sensor, updated to Version 6 (V6), provides precise ground track repeat periods for both the Terra and Aqua platforms. The LST products include daytime and nighttime surface temperature bands along with associated quality control measures such as monitoring timings, view zenith angles and clear-sky coverages as well as emissivity data from various land cover types.

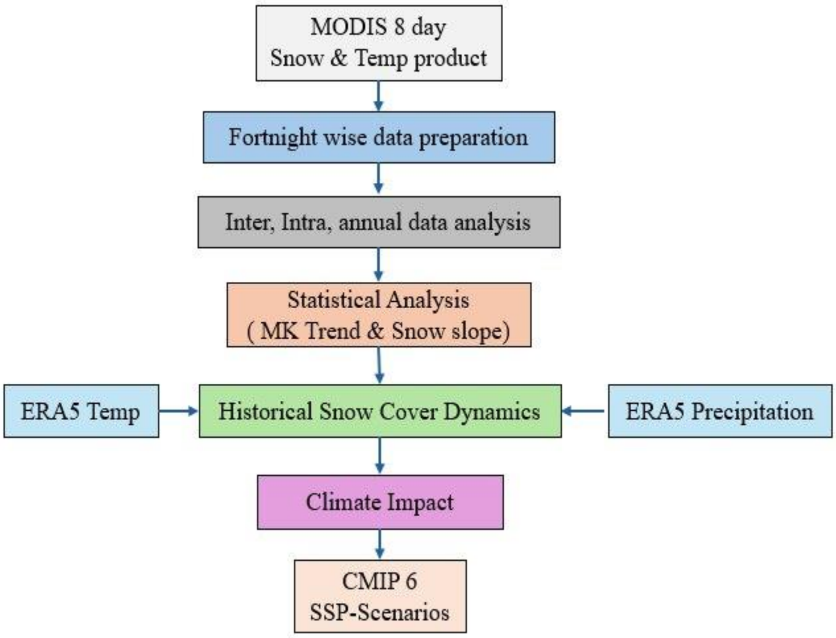

Fig. 2: Methodology Flowchart for SCA and Climate Trend Assessment

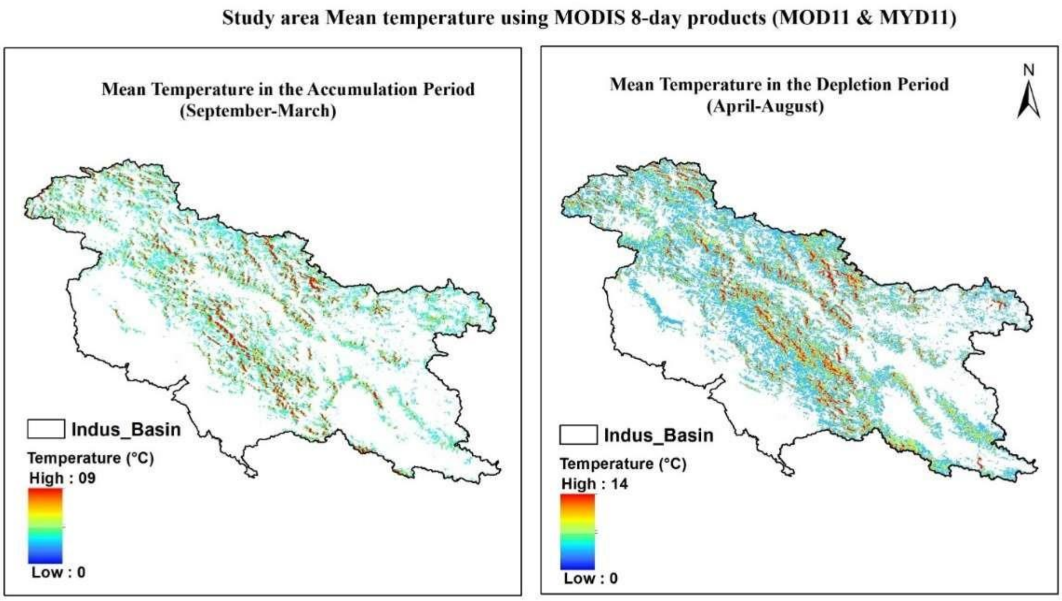

Fig. 3: Hypsometric Tinting of the Study Area Based on SRTM-DEM

Subsequently, the generated LST maps were mosaicked, projected to the WGS 84 coordinate system and clipped to the study area boundary[11]. Finally, temperature values in the maps were converted to degrees Celsius using appropriate conversion factors to facilitate further analysis and interpretation.

Statistical Analysis: Statistical methods were employed to assess the decadal variations of interannual, inter-seasonal and intra-annual trends within the study area. Various techniques were utilized including linear trend tests, the Mk and SS estimator, polynomial curve fitting and the Pearson Correlation Coefficient (PCC).

Mann-Kendall and Sen's Slope Trend Test: The trend evaluation focused on detecting patterns of increase or decrease in random variables over the study period. Non-parametric methods, including the Mann-Kendall (MK) test and Sen's robust slope estimator (SS), were selected for their effectiveness in climatology and hydrology research to identify trends and quantify rates of change[38]. The MK test and SS method were chosen following an initial comparison with Spearman rank correlation analysis. Specifically, these tests were applied to discern decadal trends in inter-annual and inter-seasonal variations of SCA within the study area[36].

The Mann-Kendall test is commonly used for long-term trend analysis in climatological and hydrological time series data. It tests the null hypothesis (H0) that there is no trend in the series against the alternative hypothesis (H1) that there is a trend. The test statistic Z_s is used to calculate the significance of the trend. If $|Z_s|$ exceeds $Z_{\alpha/2}$ (where α corresponds to the chosen significance level, e.g. 5 % with $Z_{0.025} = 1.96$), the null hypothesis is rejected, indicating a significant trend. This method is suitable for non-normally distributed time series data containing outliers and non-linear trends.

Similarly, SS estimator is a non-parametric method used to estimate the slope of a linear trend. The slope can be calculated using the following equation:

$$Q_i = \frac{x_j - x_k}{j - k}$$

where Q_i is the value of Sen's slope estimator for i = 1, 2, 3, …..N and x_j and x_k represent the data values at times j and k respectively where j > k. If N is odd, then the SS estimator is calculated as $Q_{med} = Q\ (N+1/2)$ and if N is even, then $Q_{med} = [Q_{(N/2)} + Q_{(N+1)/2)}]/2$. The slope (Q) is calculated based on data values over time intervals and Q_{med} represents the median of the SS estimator. A negative (positive) value of SS indicates a falling (rising) trend. The MK and SS tests were applied to maximum and minimum air temperatures, snow precipitation and SCA for the winter season[37].

Results from the MK test were used to analyze the presence of monotonic increasing or decreasing trends, while the SS method computed the rate of change in trends at a 95% confidence level.

Results and Discussion

Inter-annual Variability of SCA and Linear Trend: The decadal inter-annual variation of SCA revealed an average maximum SCA of 157,659.42 km² (46% of the total basin area of 342,738.02 km²) during the study period. Notably, there was a positive trend (increase) in SCA over the years, as depicted by the linear trend line[3]. The minimum annual mean SCA was observed in 2015-2016 (36.02%) followed by 2000-01 (39.22%), while the highest annual average SCA occurred in 2018-19 (53.91%), followed by 2009-10 (51.25%). Further analysis of inter-seasonal mean SCA percentage changes showed the highest coverage during winter (63.6% from December to March), followed by a gradual decrease in spring (47.86% from April to June), summer (25.9% from July to September) and autumn (39.5% in October and November).

To understand the inter-seasonal SCA trend, fortnightly annual data was analysed for winter, spring, summer and autumn on a linear trend line shown in figure 4. The study observed an increasing trend in all seasons within the NWH region-winter (0.14% per year), spring (0.35% per year), summer (0.33% per year), autumn (0.45% per year) and annually (0.35% per year). Significant fluctuations were noted in 2015-2016 and 2017-18, indicating notable changes in SCA over these years.

Similar positive trends have been documented in other studies within the Western Himalayas and HKH region, attributed to increased winter precipitation[10]. The analysis of snow cover variation over the years revealed significant fluctuations, with a noticeable increase in recent decades, as illustrated in figure 3. The study spanning the last 20 hydrological years demonstrated an overall increase in SCA across the NWH region. MK and SS tests were conducted to assess the significance of SCA trends and rate of change.

Mann-Kendall and Sen's slope test results for SCA: The MK and SS tests were conducted to assess the inter-annual trend in mean SCA % for the study period at a 95 % confidence level ($p < 0.05$). The findings of these statistical tests are summarized in table 1. The results indicate increasing insignificant trend rates for winter (Dec-Mar), summer (Jul-Sept), autumn (Oct-Nov) and annually (Sep-Aug), with rates of 0.14% $year^{-1}$, 0.33% $year^{-1}$, 0.45% $year^{-1}$ and 0.35% $year^{-1}$ respectively and corresponding Kendall attributes (Z_{mk}) of 0.74, 1.26, 1.37 and 1.89. Significantly, a positive trend was observed for Spring (Apr-Jun) at 0.26% $year^{-1}$ with a Kendall attribute (Z_{mk}) of 2.05. Similar positive trends were noted in the NWH region, particularly during the spring period.

Intra-annual variability of SCA: The mean SCA is estimated every fortnight, resulting in observations from September (first fortnight) to the following August (second fortnight) of the hydrological year. Based on the patterns of increase and decrease in SCA, the intra-annual data is categorized into an accumulation period and an ablation period[33]. During the intra-accumulation period, average SCA% changes are illustrated in figure (5a), with the highest mean observed in the first fortnight of February (70.47 %), followed by the first fortnight of March (70.15 %) and the second fortnight of March (66.14 %).

Similarly, the variation during the intra-ablation period is depicted in figure (5b), illustrating a gradual reduction in mean SCA% from the first fortnight of April to the end of the second fortnight in August. The mean minimum SCA is observed during the second fortnight of July (16.7%) and the first fortnight of August (18.2%)

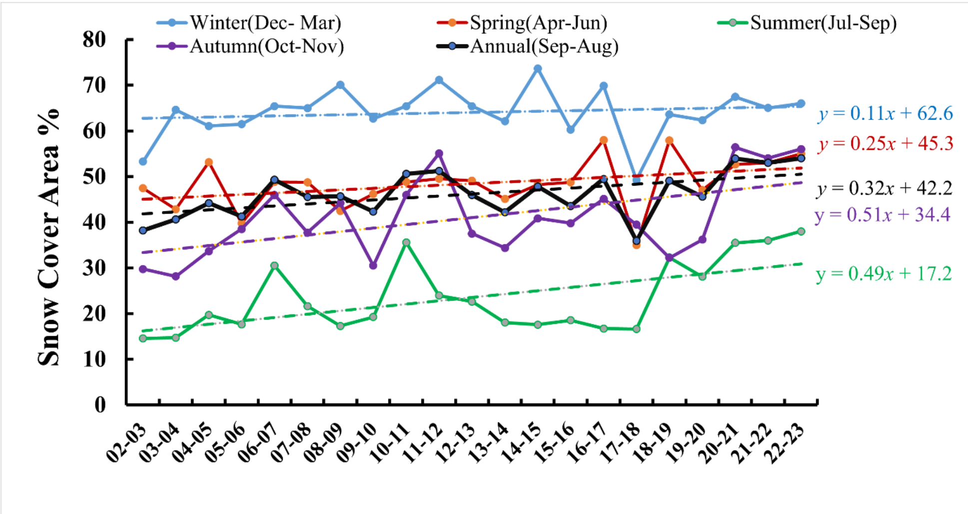

Fig. 4: Inter-seasonal SCA Trends

Table 1
Analysis of Mann-Kendall and Sen's Slope Trends

Trend Analysis	Linear Equation	Z_{mk}		Sen's slope, S
Winter (Dec-Mar)	y = 0.11x + 62.6		0.74	0.14 (% year^{-1})
Spring (Apr-Jun)	y = 0.25x + 45.3		2.05*	0.26 (% year^{-1})
Summer (Jul-Sept)	y = 0.49x + 17.2		1.26	0.33 (% year^{-1})
Autumn (Oct and Nov)	y = 0.51x + 34.4		1.37	0.45 (% year^{-1})
Annual (Sept-Aug)	y = 0.32x + 42.2		1.89	0.35 (% year^{-1})

Significant, ($p<0.005$)

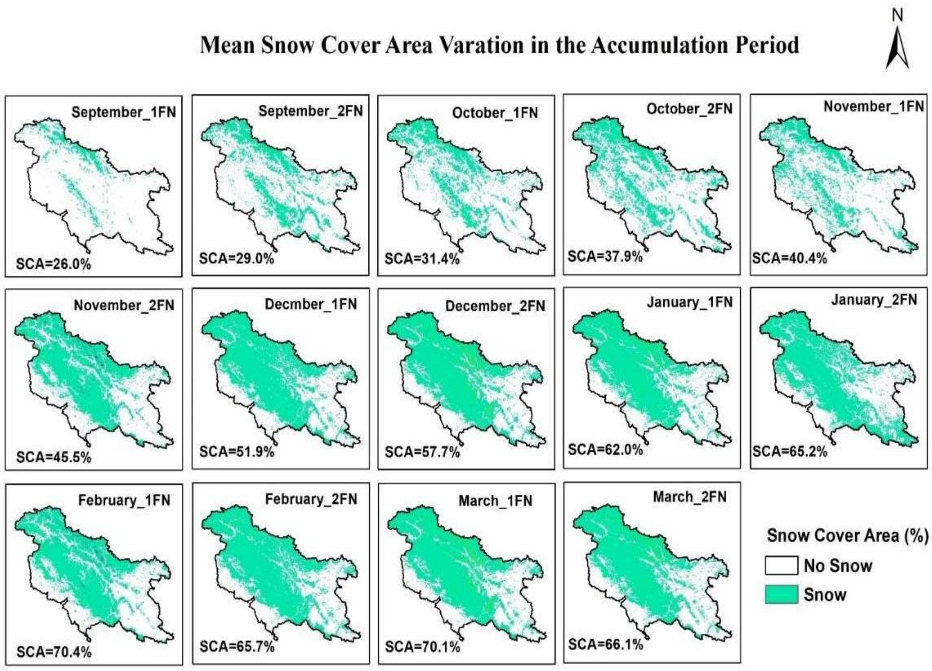

Fig. 5(a): Variation in Mean SCA% during Intra-accumulation Period (September to March)

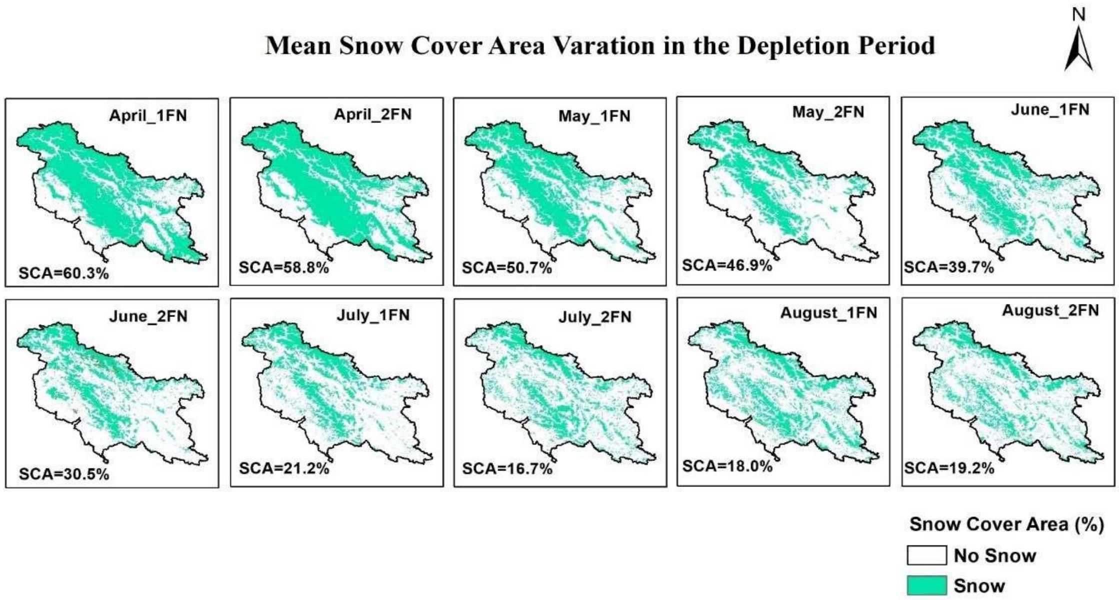

Fig. 5(b): Variation in SCA% during Intra-ablation Period

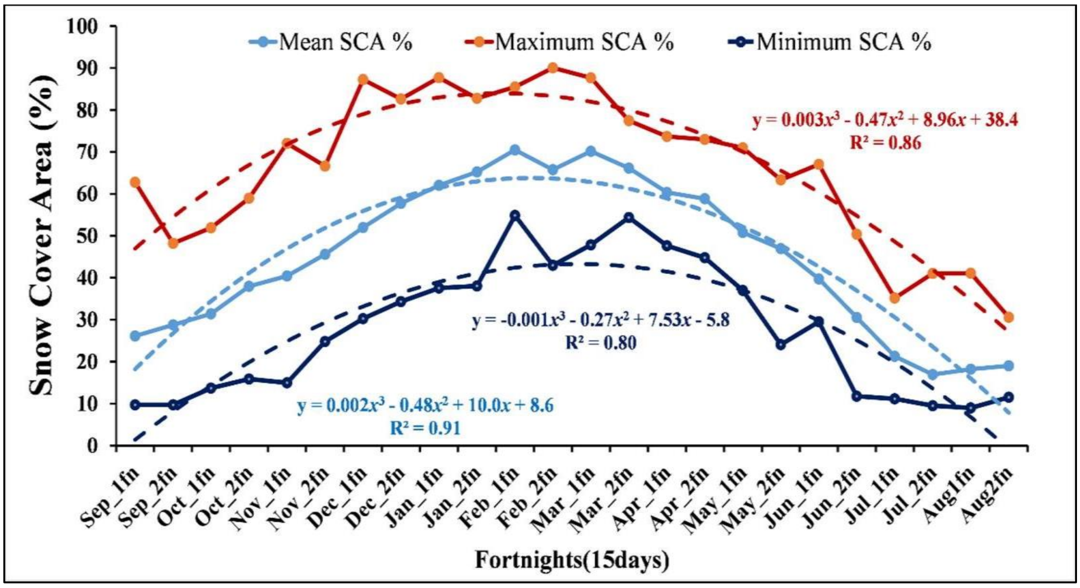

Fig. 6: Intra-annual Variations in SCA% for Mean, Maximum and Minimum

To analyze the intra-annual variations in mean, maximum and minimum SCA % throughout a hydrological year from 2002 to 2021, SCA was constructed as depicted in figure 6. These curves illustrate a gradual increase in SCA% from the first fortnight of September to the second fortnight of March, reaching its peak during this period. Conversely, a gradual decrease in SCA% is observed from the first fortnight of April to the end of the second fortnight in August. The highest SCA% recorded during the observation period was in the second fortnight of February 2012-2013 (90.06%), while the lowest SCA% was observed in the first fortnight of August 2002-2003 (8.95%). Additionally, third-order polynomial curve regressions were applied to the mean SCA%, maximum SCA% and minimum SCA%, resulting in high coefficient values of determination (R^2) of 0.91, 0.86 and 0.80 respectively as shown in figure 6.

Intra-seasonal variations of SCA on the linear trend line to investigate intra-seasonal snow cover patterns from 2002 to 2021. SCA% data were organized fortnightly for individual seasons. During the winter period (December to March), a significant increasing trend of 2.0% per fortnight was observed (Figure 7a).

Conversely, the spring period (April to May) showed a notable decreasing trend of 6.01% per fortnight (Figure 7b). In the summer period (July to August), a slight increasing trend of 0.09% per fortnight was observed (Figure 7c). The autumn period (October to November) exhibited a significant increasing trend of 4.64% per fortnight (Figure 7d), indicating the onset of snow cover accumulation in early September. By the end of August, most of the geographical area was covered by permanent snow and ice, with seasonal snow melting away.

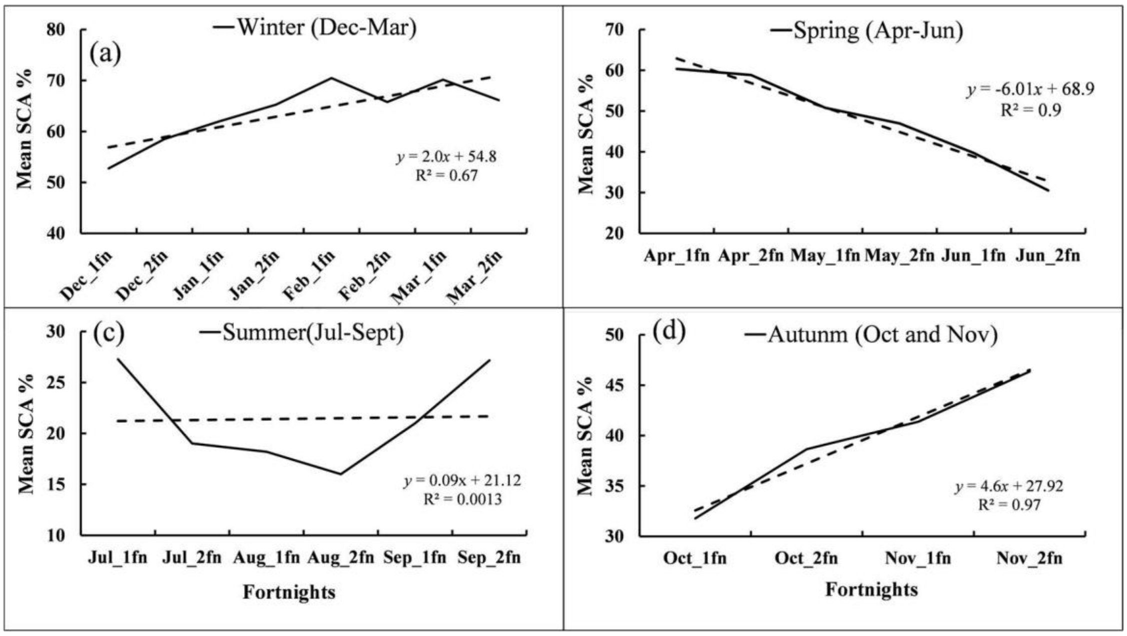

Fig. 7: Intra-seasonal SCA% variation on the linear trend line. a) Winter (Dec-Mar), b) Spring (Apr-Jun), c) Summer (Jul-Sept), d) Autumn (Oct and Nov)

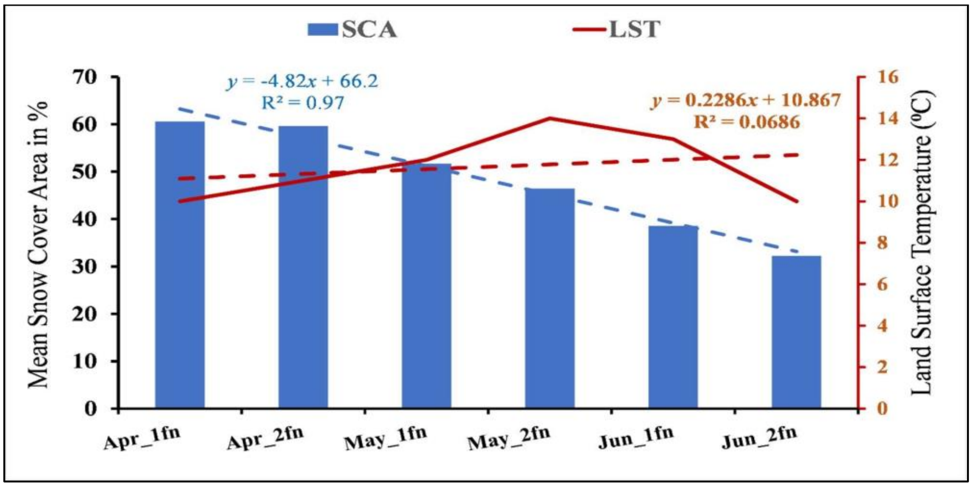

Fig. 8: Inter-relationship shown between SCA (%) and LST (^{0}C)

Climatic variability relationship between SCA and LST: The SCA exhibits a decreasing trend over time with snowmelt correlating closely with air temperature variations. Given the complex terrain of the Himalayas, a relationship was established between SCA and LST. Intra-seasonal snow cover variations were particularly noticeable during the spring period from April to June. Therefore, LST computations were focused on the period from the first fortnight of April to the second fortnight of June. The maximum LST, observed in May's first fortnight, reached 14°C while the minimum, seen in June's second fortnight, dropped to 9°C during the years 2003-2021. To assess the impacts of climatic variability on SCA % and LST in degrees Celsius, a Pearson correlation coefficient was computed for the melting period (April-June) spanning from 2003 to 2019.

The analysis revealed a notable relationship where an increase in LST corresponded to a decrease in SCA and vice versa, as depicted in figure 8. The findings indicated an insignificant negative correlation coefficient of 0.81 at the 0.05 significance level (2-tailed), suggesting an inverse relationship between LST and SCA. Similar observations have been noted in previous studies where high rainfall in the Kashmir valley correlated with periods of low temperatures and vice versa. Additionally, during the spring season, the LST exhibited a trend increase of 0.2°C per fortnight while the SCA declined by 4.82% per fortnight.

SCA relation with Elevation Zones: The average elevation of the Indus basin was determined to be 4200 Masl based on the hypsometric curve derived from the study area's digital elevation model (DEM). The study area was divided into nine distinct elevation zones, each spanning 1000 meters. This zoning was carried out to investigate how topographic altitude influences snow coverage variation. The hypsometric curve illustrates (Fig. 9) that most of the basin area (> 40%) is situated between 4000 and 5000 meters.

Mann-Kendall and Sen's slope test results for Zone wise SCA: The MK and SS estimators are robust statistical methods employed to analyze trends in environmental data, such as SCA. In this study, these techniques were utilized to evaluate SCA trends across various elevation zones within the study area. The findings from these analyses yield important insights into how snow cover varies with altitude, illuminating the influence of elevation on snow extent trends. Notably, zones 1, 2 and 3 (lower elevation zones) exhibit a significant decreasing trend in SCA with rates ranging from -0.13% to -0.31% per year. Conversely, higher elevation zones (Zones 4 to 8) demonstrate positive increment trends in SCA, with rates exceeding 0.23% per year. These results underscore the intricate relationship between elevation and snow cover dynamics, offering valuable insights into how environmental factors shape SCA variations.

Assessing climatic variability trends using ECMWF ERA5: Re-analysis for total precipitation understanding climatic variability, especially regarding precipitation trends, is essential for assessing climate change impacts. Re-analysis data such as ECMWF ERA5, offers valuable insights into long-term precipitation patterns. The ECMWF ERA5 reanalysis data for total precipitation over the selected time period reveals a statistically significant decreasing trend of 0.016% per year as illustrated in figure 10.

Climate change projections in the study area: In anticipation of future climate conditions in the Indus Himalayas, this analysis delves into the projected trends of annual temperatures, leveraging historical data from 1995-2014 to extrapolate trends up to the year 2100.

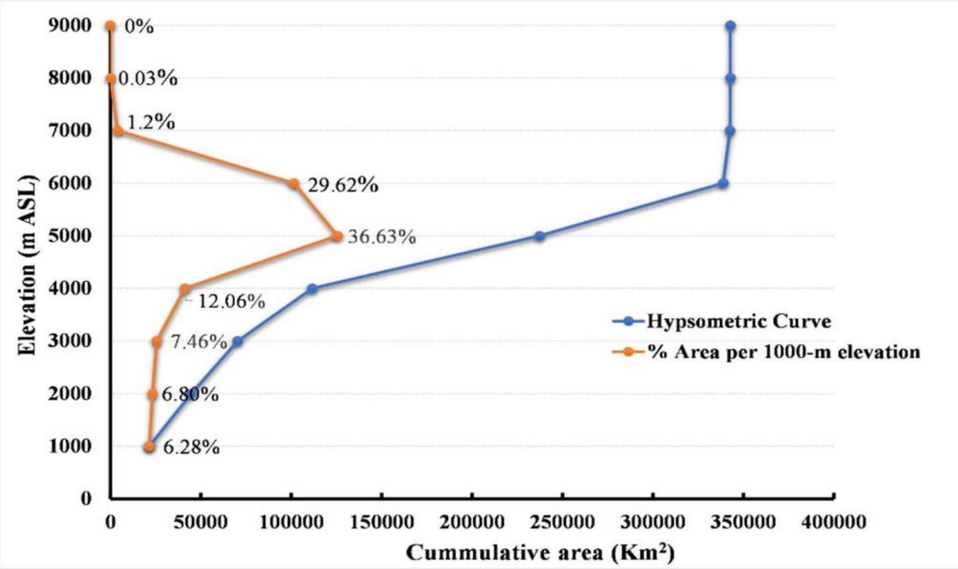

Fig. 9: Elevation Range and Proportional Area (%) of Each Zone. Snow Coverage Analysis

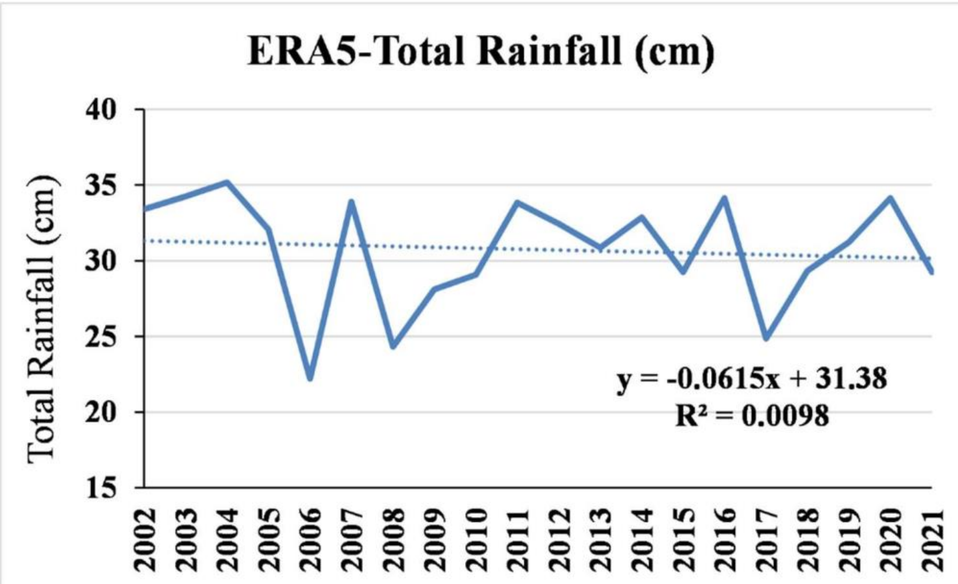

Fig. 10: Total Precipitation Linear Trend over a time period.

Table 2
Trend analysis of SCA across elevation zones

Trend Analysis	Linear Equation	Zmk	Sen's slope, S
Zone 1 (1000-2000)	y = 0.10x + 61.3	0.34	-0.31 (%year^{-1})
Zone 2 (2000-3000)	y = 0.15x + 45.3	2.05*	-0.20 (%year^{-1})
Zone 3 (3000-4000)	y = 0.39x + 16.2	1.08	-0.13 (%year^{-1})
Zone 4 (4000-5000)	y = 0.51x + 34.4	1.03	0.35 (%year^{-1})
Zone 5 (5000-6000)	y = 0.22x + 42.1	1.89	0.45 (%year^{-1})
Zone 6 (6000-7000)	y = 0.15x + 45.3	2.08*	0.3 (%year^{-1})
Zone 7 (7000-8000)	y = 0.11x + 35.3	2*	0.23 (%year^{-1})
Zone 8 (>8000)	y = 0.8x + 23.3	1.8*	0.12 (%year^{-1})

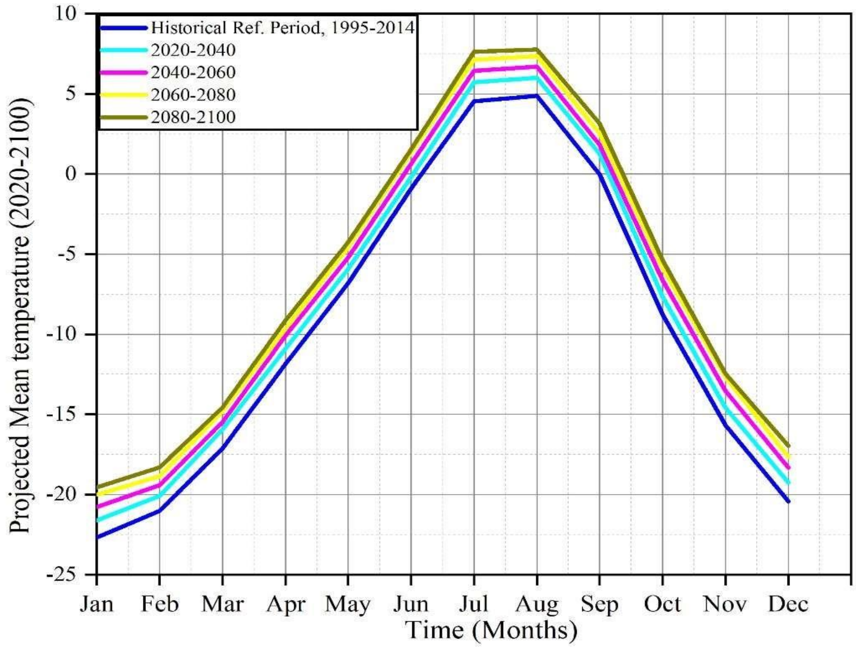

Fig. 11: Projected Mean Temperature (2020-2100) - SSP2_4.5

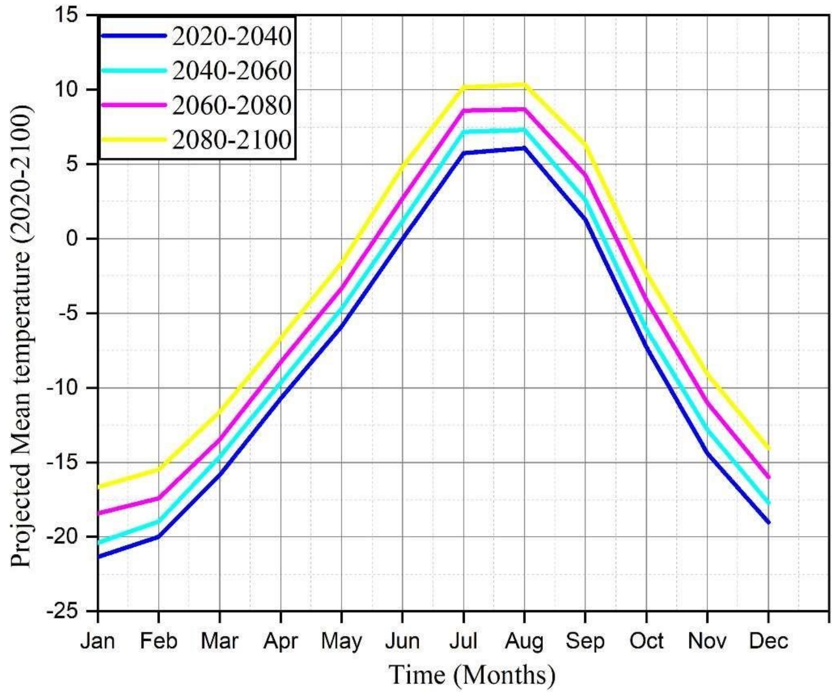

Fig. 12: Projected Mean Temperature (2020-2100) - SSP5_8.5

By segmenting the analysis into four distinct time periods (2020-2040, 2040-2060, 2060-2080 and 2080-2100) and considering different climate scenarios outlined by Shared Socioeconomic Pathways (SSP1-2.6, SSP2-4.5 and SSP5-8.5), this study offers invaluable insights into potential temperature shifts. Under SSP2-4.5, for instance, January temperatures are expected to gradually decrease from -22.67°C (historical reference) to -19.55°C by 2100.

In contrast, projections under SSP5-8.5 depict more pronounced increases, with January temperatures ranging from -21.35°C (2020-2040) to 16.66°C (2080-2100). The detailed forecasts for each month and time period provide a comprehensive view of future temperature variations, crucial for informed decision-making and climate adaptation strategies. Figures 11 and 12 highlight the projected mean temperatures under SSP2-4.5 and SSP5-8.5 respectively illustrating the significant implications of different climate scenarios on regional temperatures. Additionally, figure 13 offers a comparative analysis of annual projected temperatures across historical and SSP-driven periods, emphasizing the importance of considering diverse climate projections for effective disaster preparedness and long-term planning in the Indus Himalayas.

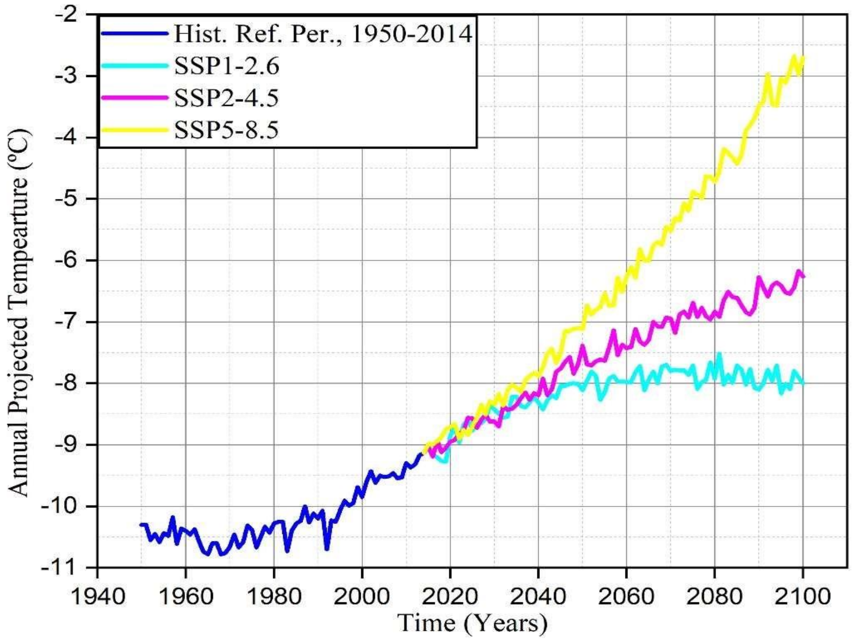

Fig. 13: Annual Projected Temperature (°C) - Historical V_s. SSP Scenarios

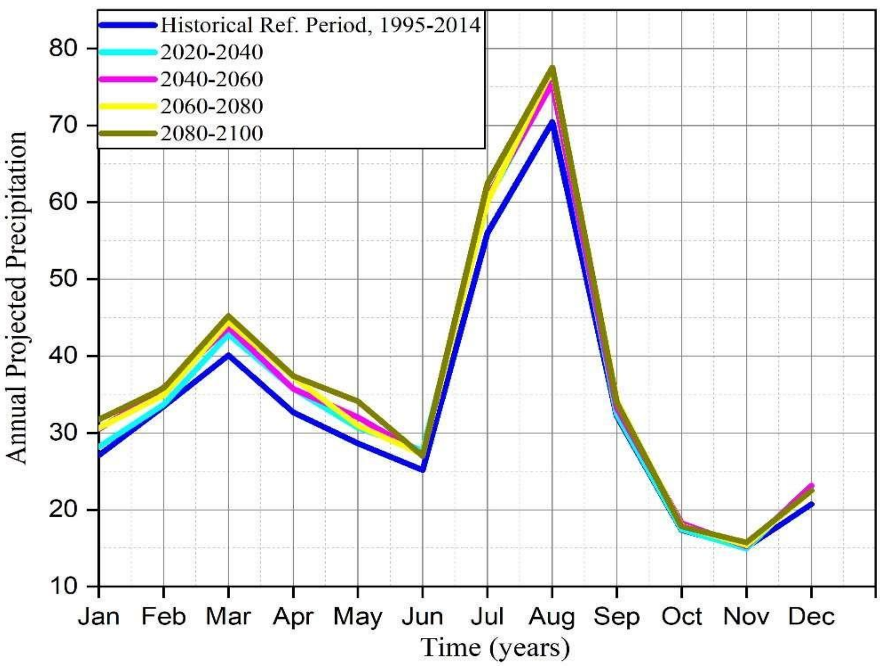

Fig. 14: Annual Precipitation Trends

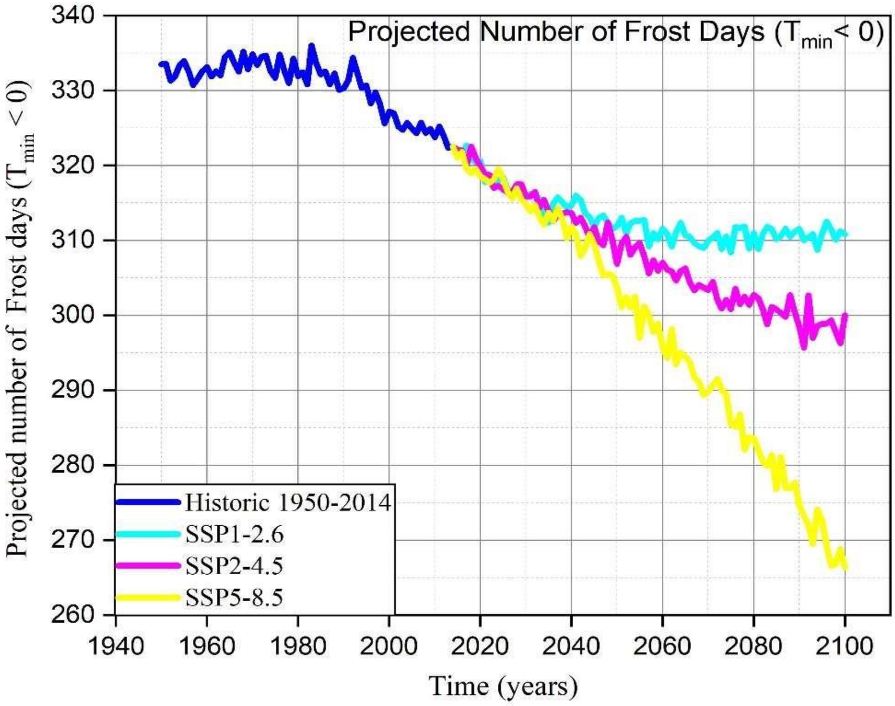

Fig. 15: Annual Frost Days Trends

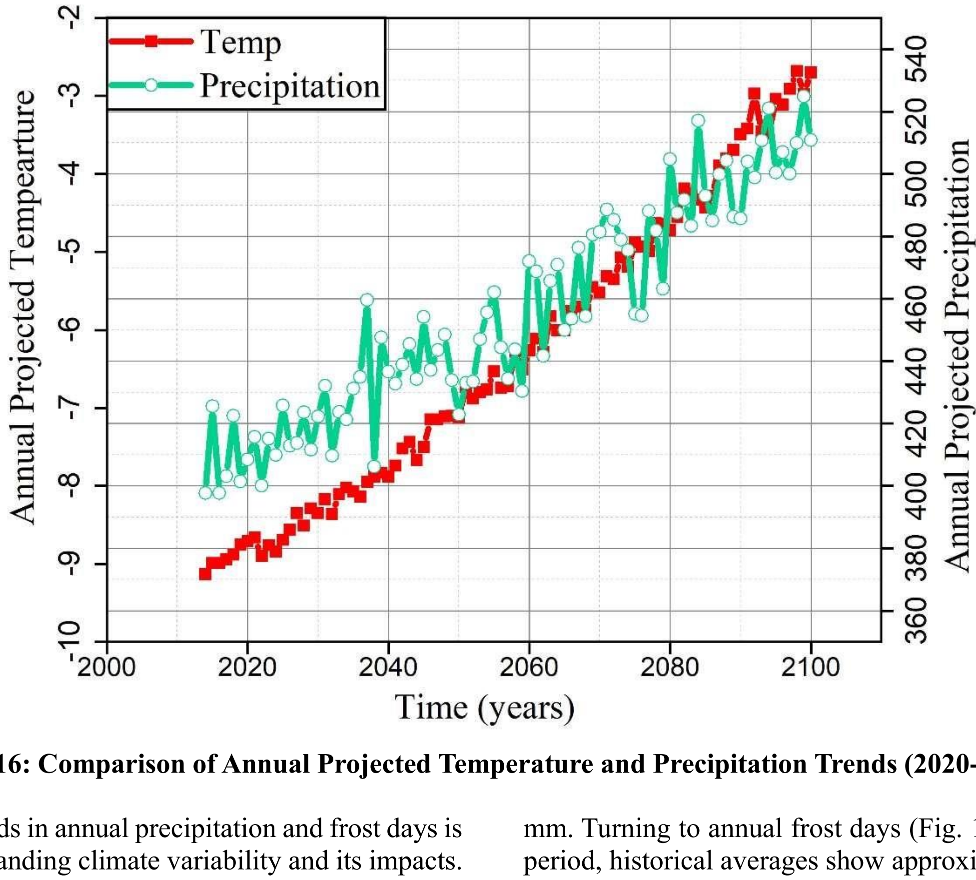

Fig. 16: Comparison of Annual Projected Temperature and Precipitation Trends (2020-2100)

Analyzing the trends in annual precipitation and frost days is crucial for understanding climate variability and its impacts. The historical data from 1950 to 2014 (Fig. 14) indicates an average annual precipitation of approximately 392.15 mm, showing notable variability over time. Looking ahead to future scenarios under SSP1-2.6, SSP2-4.5 and SSP5-8.5, we see projected changes in precipitation levels. By 2010, under SSP2-4.5, precipitation is expected to reach 415.91 mm. Turning to annual frost days (Fig. 15) during the same period, historical averages show approximately 333.51 days annually, reflecting seasonal variations.

Future projections suggest a decline in frost days, particularly under SSP5-8.5 where the number of frost days is expected to decrease to 266.37 by 2100. These figures highlight significant shifts in precipitation and frost days, emphasizing their importance for assessing climate impacts on ecosystems, agriculture and water resources. The comparison graph depicted in figure 16 illustrates the trends in annual projected temperature and precipitation from 2020 to 2100. This graph provides valuable insights into the expected changes in temperature and precipitation over the course of this century. The data for this comparison is based on scenarios SSP1-2.6, SSP2-4.5 and SSP5-8.5, offering a comprehensive view of potential future climatic conditions.

Conclusion

This study underscores the significant role of climate variability in shaping snow cover dynamics and hydrological processes in the NWH region. Innovative techniques like the multi-image combination method have enhanced the usability of snow cover data, crucial for hydrological assessments in complex terrains. The analysis identifies distinct seasonal trends in SCA. While winter, summer and autumn exhibit marginal, statistically insignificant increases in SCA (0.14% $year^{-1}$, 0.33% $year^{-1}$ and 0.45% $year^{-1}$ respectively), a noteworthy positive trend is observed in spring (0.35% $year^{-1}$). Additionally, the study investigates the relationship between elevation zones and SCA trends, revealing a significant decreasing trend in lower elevation zones (1000-3000 meters) and a notable increasing trend in higher elevation zones (>4000 meters), illustrating the intricate elevation-snow dynamics within the NWH region.

Temperature emerges as a critical driver influencing SCA changes during melting periods, with an observed increase over the study period. The study also notes a decreasing trend in annual frost days, indicative of rising temperatures in the region. These findings underscore the dynamic nature of climate impacts on snow cover and hydrology. The integration of future climate projections until 2100 including temperature changes, precipitation patterns and annual frost days ($T_{min} < 0$), provides vital insights for disaster preparedness and resilience-building in the Indus Himalayas. Understanding evolving climate dynamics and snow cover trends is imperative for formulating targeted strategies to mitigate environmental risks and to ensure the long-term sustainability of communities in the region.

References

1. Banerjee A., Kang S., Meadows M.E., Xia Z., Sengupta D. and Kumar V., Quantifying climate variability and regional anthropogenic influence on vegetation dynamics in northwest India, *Environmental Research*, **234**, 116541 **(2023)**

2. Barnett T.P., Adam J.C. and Lettenmaier D.P., Potential impacts of a warming climate on water availability in snow-dominated regions, *Nature*, **438(7066)**, 303-309 **(2005)**

3. Bhardwaj N., Nikam B.R., Yadav S.K.S., Shukla S., Mohapatra M., Aggarwal S.P. and Poddar J., Snow Cover Mapping Over the Region of Hindu Kush Himalaya (HKH) for 2008–2018 Using Cloud Mitigated Moderate Resolution Spectroradiometer (MODIS) Snow Cover Data, In Sustainable Infrastructure Development: Select Proceedings of ICSIDIA 2020, Singapore, Springer Singapore, 105-115 **(2022)**

4. Bolch T., Kulkarni A., Kääb A., Huggel C., Paul F., Cogley J.G., Frey H., Kargel J.S., Fujita K., Scheel M. and Bajracharya S., The state and fate of Himalayan glaciers, *Science*, **336(6079)**, 310-314 **(2012)**

5. Desinaya K.N., Prasad A.K., El-Askary H., Kafatos M. and Asrar G.R., Snow cover variability and trend over the Hindu Kush Himalayan region using MODIS and SRTM data, In Annales Geophysicae, Copernicus GmbH, **40(1)**, 67-82 **(2022)**

6. Dharpure J.K., Goswami A., Patel A., Kulkarni A.V. and Snehmani, Assessment of snow cover variability and its sensitivity to hydrometeorological factors in the Karakoram and Himalayan region, *Hydrological Sciences Journal*, **66(15)**, 2198-2215 **(2021)**

7. Dharpure J.K., Patel A., Goswami A., Kulkarni A.V. and Snehmani, Spatiotemporal snow cover characterization and its linkage with climate change over the Chenab river basin, western Himalayas, *GI Science & Remote Sensing*, **57(7)**, 882-906 **(2020)**

8. Dimri A.P., Niyogi D., Barros A.P., Ridley J., Mohanty U.C., Yasunari T. and Sikka D.R., Western Disturbances: A review, *Reviews of Geophysics*, **53(2)**, 225–246 **(2015)**

9. Faiz M.A., Liu D., Tahir A.A., Li H., Fu Q., Adnan M., Zhang L. and Naz F., Comprehensive evaluation of 0.25° precipitation datasets combined with MOD10A2 snow cover data in the ice-dominated river basins of Pakistan, *Atmospheric Research*, **231**, 104653 **(2020)**

10. Gao Y., Xie H., Yao T. and Xue C., Integrated assessment on multi-temporal and multi-sensor combinations for reducing cloud obscuration of MODIS snow cover products of the Pacific Northwest USA, *Remote Sensing of Environment*, **114(8)**, 1662–1675 **(2010)**

11. Hammond J.C., Saavedra F.A. and Kampf S.K., Global snow zone maps and trends in snow persistence 2001–2016, *International Journal of Climatology*, **38(12)**, 4369–4383 **(2018)**

12. Haq M.A., Baral P., Yaragal S. and Rahaman G., Assessment of trends of land surface vegetation distribution, snow cover and temperature over entire Himachal Pradesh using MODIS datasets, *Natural Resource Modeling*, **33(2)**, e12262 **(2020)**

13. Hasan M.R. and Pattnaik S., Characteristics of Western Disturbance intensification and associated induced circulations over the Indian Region, *Natural Hazards Research*, **4(3)**, 486-497 **(2023)**

14. Huang X., Liang T., Zhang X. and Guo Z., Validation of MODIS snow cover products using Landsat and ground measurements during the 2001–2005 snow seasons over northern Xinjiang, China, *International Journal of Remote Sensing*, **32(1)**, 133-152 **(2011)**

15. Jabin G., Dolker S., Joshi B.D., Singh S.K., Chandra K., Sharma L.K. and Thakur M., Lahaul–Zanskar–Sham valley corridor in Indian trans Himalayan region facilitates dispersal and gene flow in Himalayan ibex, *Biology*, **12(3)**, 382 **(2023)**

16. Jiang Y., Du W., Chen J. and Sun W., Spatiotemporal Variations in Snow Cover and Hydrological Effects in the Upstream Region of the Shule River Catchment, Northwestern China, *Remote Sensing*, **13(16)**, 3212 **(2021)**

17. Krishna A.P. and Sharma A., October. Snow cover and land surface temperature assessment of Gangotri basin in the Indian Himalayan Region (IHR) using MODIS satellite data for climate change inferences, In Earth resources and environmental remote sensing/GIS applications IV, SPIE, **8893**, 273-281 **(2013)**

18. Kulkarni A.V., Rathore B.P. and Singh S.K., Distribution of seasonal snow cover in central and western Himalaya, *Annals of Glaciology*, **51(54)**, 123-128 **(2010)**

19. Kumar D., Thind P.S. and Sharma T., Impacts of changing climate and topography on snow cover variability of Parvati River Basin, western Himalayas, India, *Environmental Science and Pollution Research*, **31(1)**, 1007-1025 **(2024)**

20. Laghari A.N., Vanham D. and Rauch W., To what extent does climate change result in a shift in Alpine hydrology? A case study in the Austrian Alps, *Hydrological Sciences Journal*, **57(1)**, 103-117 **(2012)**

21. Misra A., Kumar A., Bhambri R., Haritashya U.K., Verma A., Dobhal D.P., Gupta A.K., Gupta G. and Upadhyay R., Topographic and climatic influence on seasonal snow cover: Implications for the hydrology of ungauged Himalayan basins, India, *Journal of Hydrology*, **585**, 124716 **(2020)**

22. Nautiyal S., Goswami M., Prakash S., Rao K.S., Maikhuri R.K., Saxena K.G., Baksi S. and Banerjee S., Spatio-temporal variations of geo-climatic environment in a high-altitude landscape of Central Himalaya: An assessment from the perspective of vulnerability of glacial lakes, *Natural Hazards Research*, **2(4)**, 343-362 **(2022)**

23. Qiao H. and Zhang Y., FY-3C and FY-4A satellite data were combined to study the variation of snow cover area: A case study of Qilian Mountains, *Remote Sensing Technology and Application*, **35(6)**, 1320-1328 **(2020)**

24. Rasheed M.U., Mahmood S.A., Khan R.M.A. and Sohl M.A., LS8pyCalc: semi-automated Python calculator to retrieve land surface temperature, cross verified through in situ and MODIS datasets, *Arabian Journal of Geosciences*, **16(11)**, 627 **(2023)**

25. Reddy G.P.O., Kumar N., Sahu N., Srivastava R., Singh S.K., Naidu L.G.K., Chary G.R., Biradar C.M., Gumma M.K., Reddy B.S. and Kumar J.N., Assessment of spatio-temporal vegetation dynamics in tropical arid ecosystem of India using MODIS time-series vegetation indices, *Arabian Journal of Geosciences*, **13**, 1-13 **(2020)**

26. Saavedra F. A., Kampf S.K., Fassnacht S.R. and Sibold J.S., Changes in Andes snow cover from MODIS data, 2000-2016, *Cryosphere*, **12(3)**, 1027–1046 **(2018)**

27. Sahu R. and Gupta R.D., Snow cover analysis in Chandra Basin of Western Himalaya from 2001 to 2016, In Applications of Geomatics in Civil Engineering: Select Proceedings of ICGCE 2018, Springer Singapore, 557-566 **(2020)**

28. Sharma A., Bhattacharya A. and Venkataraman C., Influence of aerosol radiative effects on surface temperature and snow melt in the Himalayan region, *Science of the Total Environment*, **810**, 151299 **(2022)**

29. Singh S., Tiwari R.K., Sood V. and Gusain H.S., Detection and validation of spatiotemporal snow cover variability in the Himalayas using Ku-band (13.5 GHz) SCATSAT-1 data, *International Journal of Remote Sensing*, **42(3)**, 805-815 **(2021)**

30. Singh S.K., Rathore B.P., Bahuguna I.M. and Ajai, Snow cover variability in the Himalayan–Tibetan region, *International Journal of Climatology*, **34(2)**, 446-452 **(2014)**

31. Supriya V.M., Rao B.S., Krishna C.S., Raju P.V. and Rao V.V., Spatio-Temporal Variability Analysis of Snow Cover in Sutlej Basin Using MODIS Snow Cover Data, In Hydrology and Hydrologic Modelling, Proceedings of 26th International Conference on Hydraulics, Water Resources and Coastal Engineering (HYDRO 2021), **312(1)**, 293 **(2023)**

32. Tang B.H., Shao K., Li Z.L., Wu H., Nerry F. and Zhou G., Estimation and validation of land surface temperatures from Chinese second-generation polar-orbit FY-3A VIRR data, *Remote Sensing*, **7(3)**, 3250-3273 **(2015)**

33. Virdis S.G., Soodcharoen N., Lugliè A. and Padedda B.M., Estimation of satellite-derived lake water surface temperatures in the western Mediterranean: Integrating multi-source, multi-resolution imagery and a long-term field dataset using a time series approach, *Science of the Total Environment*, **707**, 135567 **(2020)**

34. Yadav J.S., Tiwari S.K., Misra A., Rai S.K. and Yadav R.K., High-altitude meteorology of Indian Himalayan Region: complexities, effects and resolutions, *Environmental Monitoring and Assessment*, **193**, 1-29 **(2021)**

35. Yadav S.K. and Borana S.L., MODIS derived NDVI based time series analysis of vegetation in the Jodhpur area, *The International Archives of the Photogrammetry, Remote Sensing and Spatial Information Sciences*, **42**, 535-539 **(2019)**

36. Yang D., Wang W. and Hong T., A historical weather forecast dataset from the European Centre for Medium-Range Weather Forecasts (ECMWF) for energy forecasting, *Solar Energy*, **232**, 263-274 **(2022)**

37. Yao R., Wang L., Wang S., Wang L., Wei J., Li J. and Yu D., A detailed comparison of MYD11 and MYD21 land surface temperature products in mainland China, *International Journal of Digital Earth*, **13(12)**, 1391-1407 **(2020)**

38. Yu P., Zhao T., Shi J., Ran Y., Jia L., Ji D. and Xue H., Global spatiotemporally continuous MODIS land surface temperature dataset, *Scientific Data*, **9(1)**, 143 **(2022)**.

(Received 15th May 2024, accepted 19th July 2024)